Polarized Dust Emission × Neutral Hydrogen

George Halal
Stanford University

CMB-S4 Collaboration Meeting
August 2, 2023

1. BICEP / *Keck* XVI: Characterizing Dust Polarization Through Correlations with Neutral Hydrogen (BICEP/Keck Collaboration et al., *ApJ*, 2023)

2. Filamentary Dust Polarization and the Morphology of Neutral Hydrogen Structures

(Halal, Clark, Cukierman, Beck, & Kuo, submitted to *ApJ*, 2023)

Polarized Dust Emission

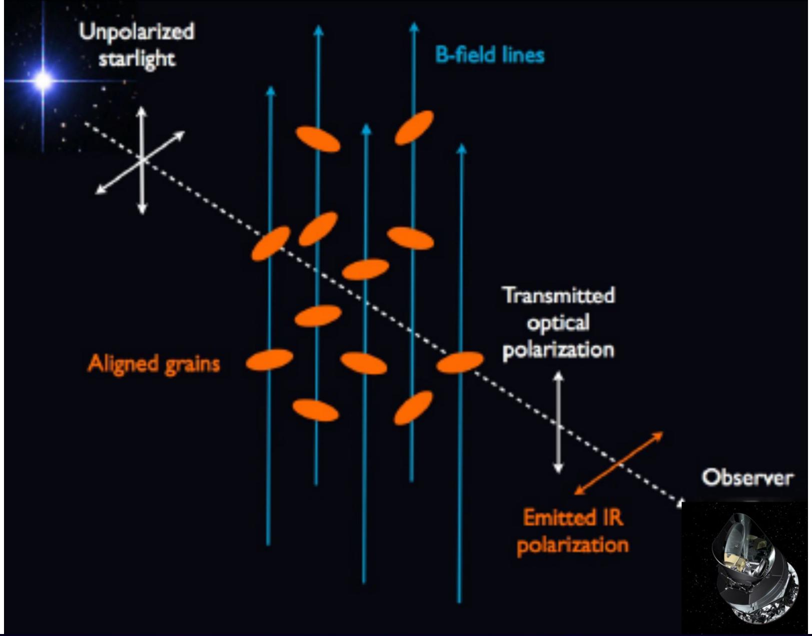

CMB Foreground

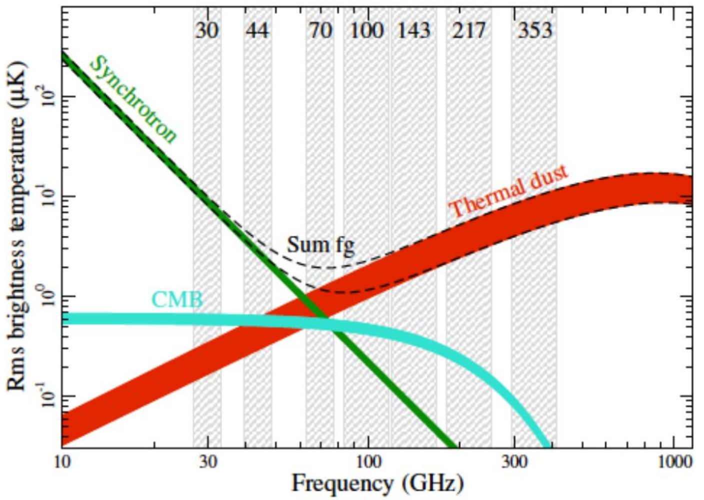

Neutral Hydrogen (HI)

well-mixed with dust + filamentary + aligned with magnetic field + 3D

Rolling Hough Transform

HI intensity → HI filaments → Magnetic field orientation → HI-based polarization template

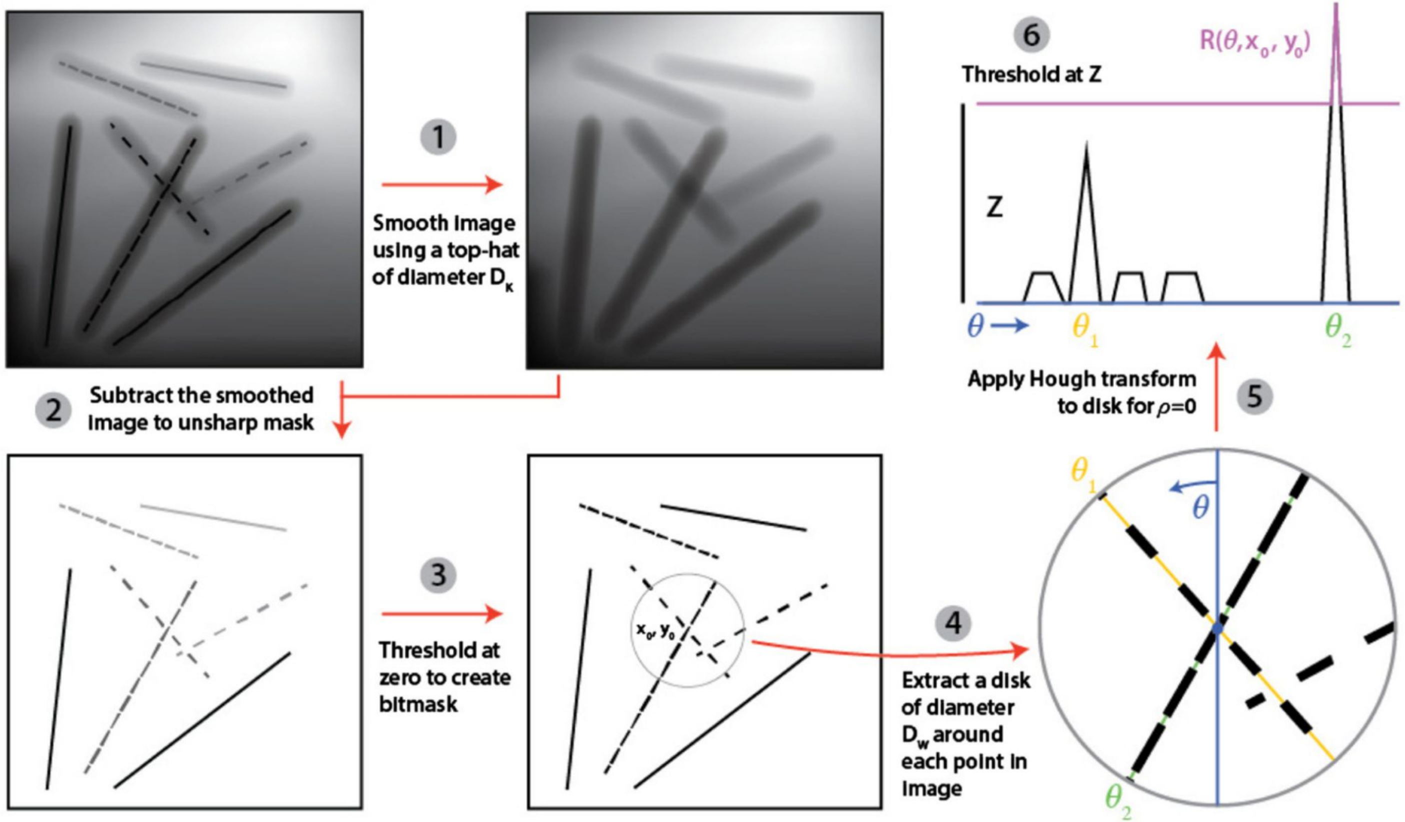

Clark, et al. (2014)

Clark & Hensley (2019)

Background: 1st moment map of velocity
Texture: magnetic field orientation inferred by HI filaments

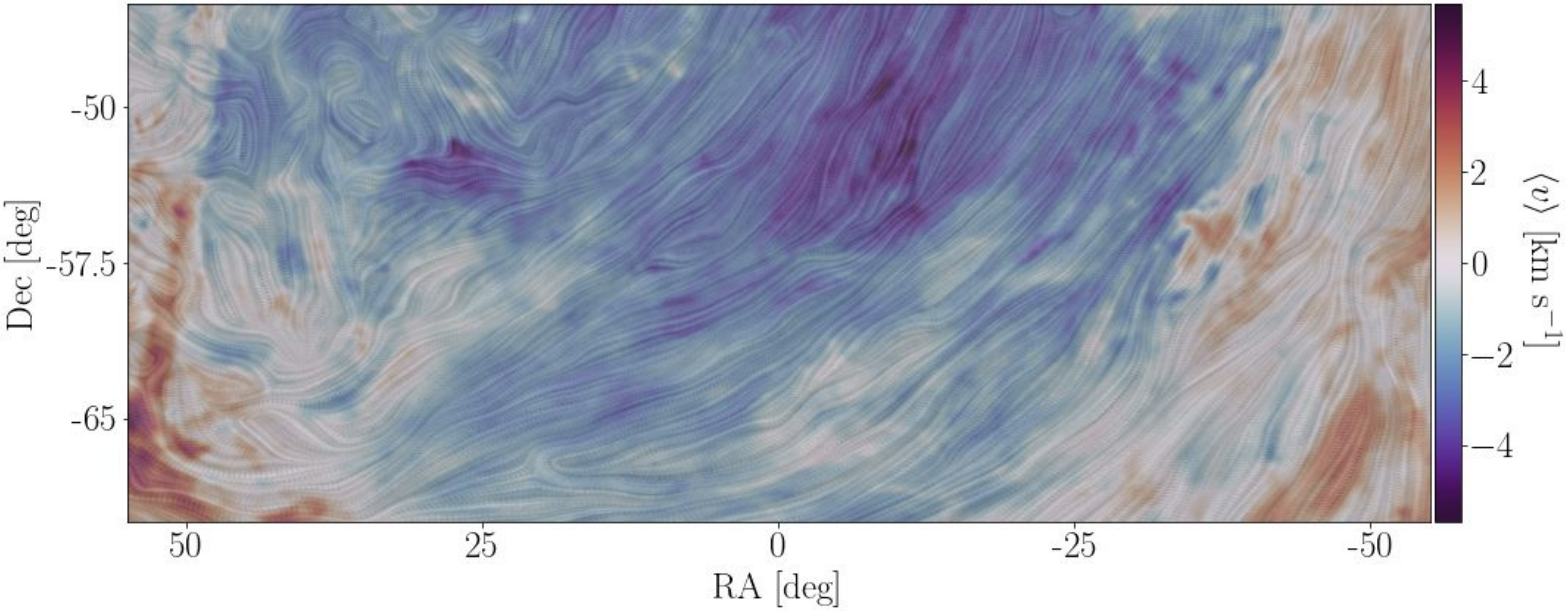

Polarized emission in velocity components

BICEP/Keck Collaboration et al., *ApJ*, 2023

- Detection in the Galactic component of HI → down to 95 GHz
  ~7σ in BB, ~15σ in EE, and ~16σ in EE+BB

- No detection in Magellanic Stream I

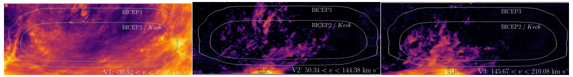

	V1	V2	V3	V2 + V3
BB	6.7	1.3	0.6	0.9
EE	14.6	2.4	1.4	2.5
$BB + EE$	16.1	1.6	1.2	0.3

No evidence for decorrelation in BICEP

BICEP/Keck Collaboration et al., *ApJ*, 2023

- No evidence for LOS frequency decorrelation from inclusion of IVC in LOS sum
- Fit an SED:
  no decorrelation between filaments and total dust

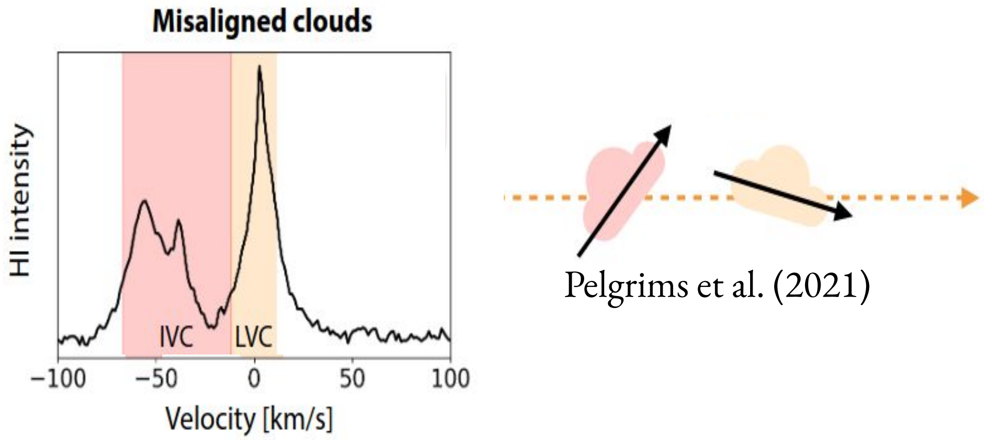

Pelgrims et al. (2021)

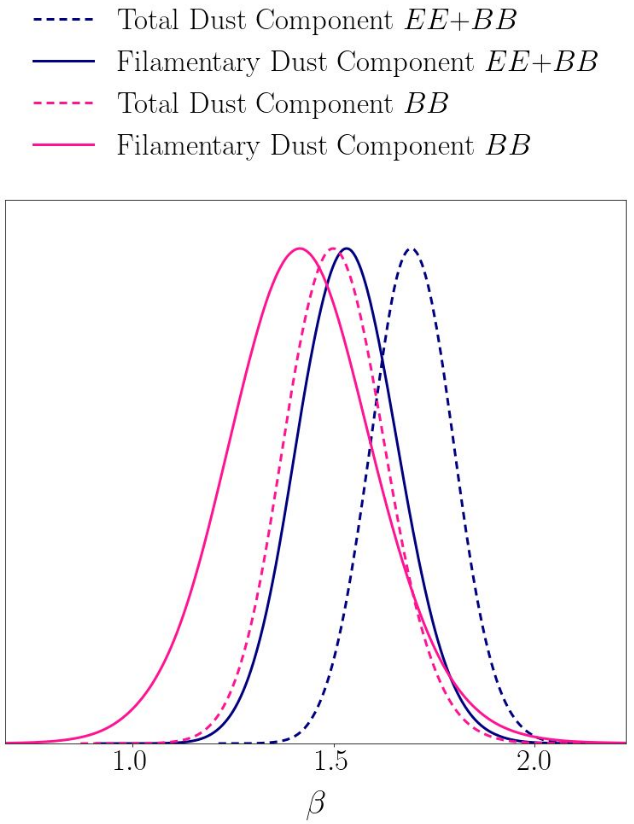

Dust sensitivity of different instruments

BICEP/Keck Collaboration et al., *ApJ*, 2023

	BB	EE	$BB + EE$
BICEP3 95 GHz	4.53	1.22	4.72
Planck 143 GHz	0.05	0.72	0.12
BICEP2/*Keck* 150 GHz	5.31	2.43	5.98
Planck 217 GHz	3.50	2.37	4.02
Keck 220 GHz	5.82	7.13	9.26
Planck 353 GHz	3.18	7.99	8.59

Statistical significance of detection of HI-based polarization template in units of standard deviations

New RHT implementation using spherical harmonic convolutions

Halal, Clark, Cukierman, Beck, & Kuo,
submitted to *ApJ*, 2023

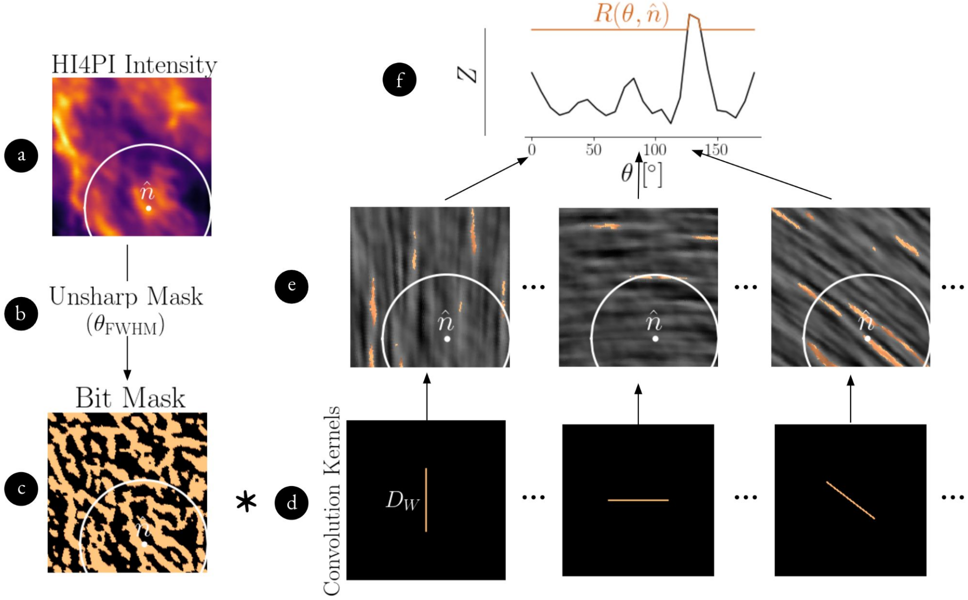

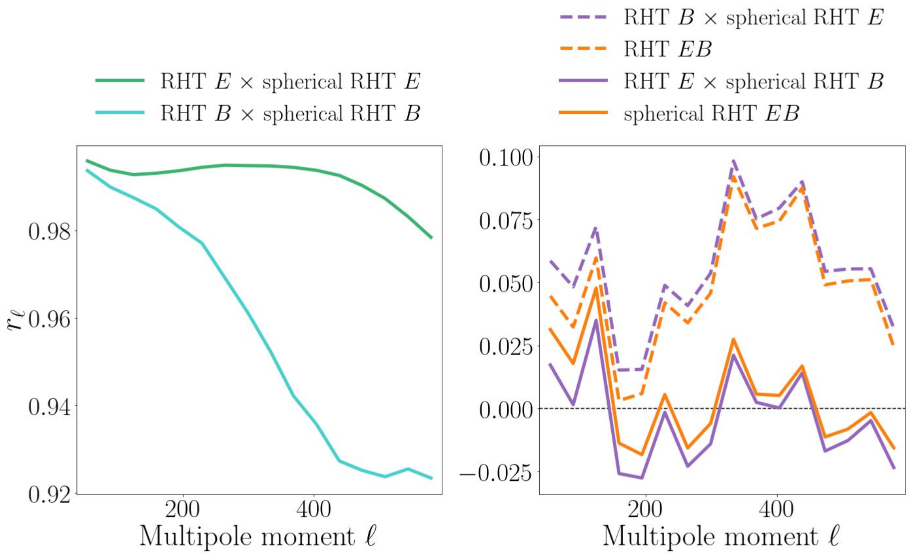

Explore filament morphologies

Halal, Clark, Cukierman, Beck, & Kuo, submitted to *ApJ*, 2023

Thinnest resolved filaments most informative for magnetic field modeling

Also: ~10% enhancement in *B*-mode correlation with higher resolution HI data

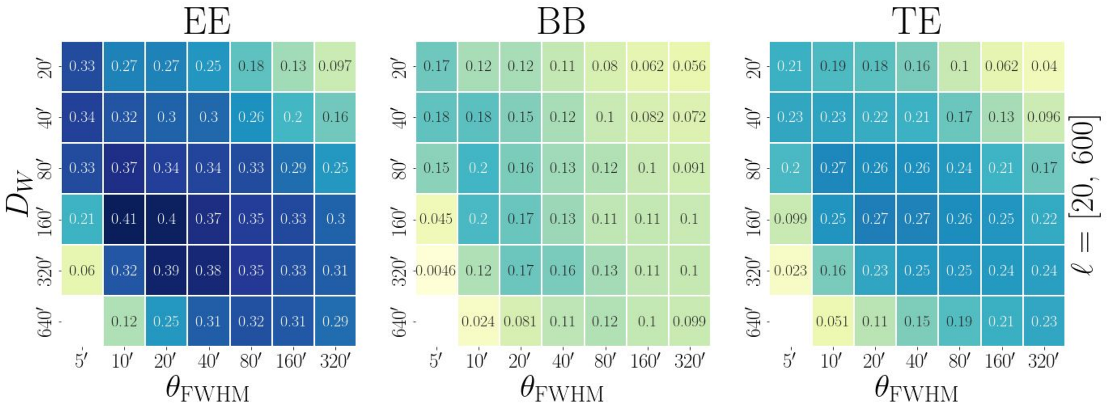

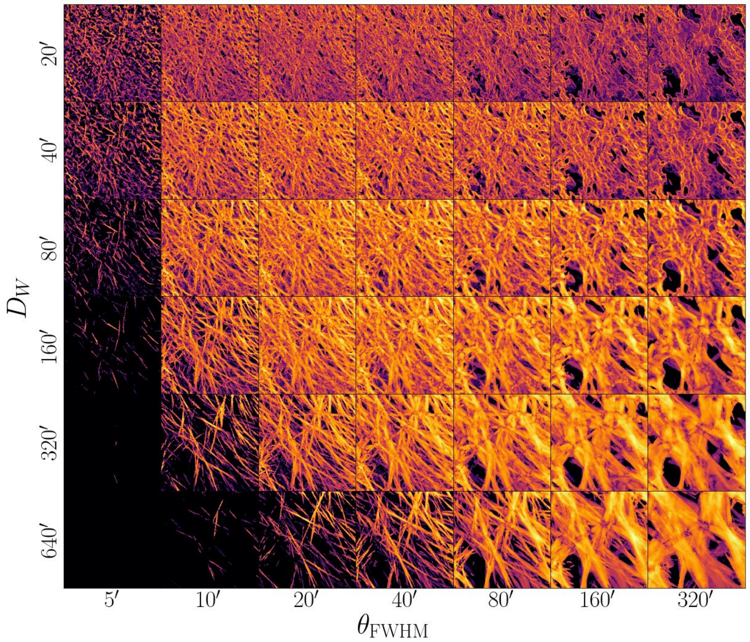

Morphologies producing *TB*, *EB* > 0

Halal, Clark, Cukierman, Beck, & Kuo, submitted to *ApJ*, 2023

Even under assumption of local B-field alignment

B modes mostly affected by: Filament topologies wrt one another
E modes mostly sensitive to: Individual filament shapes

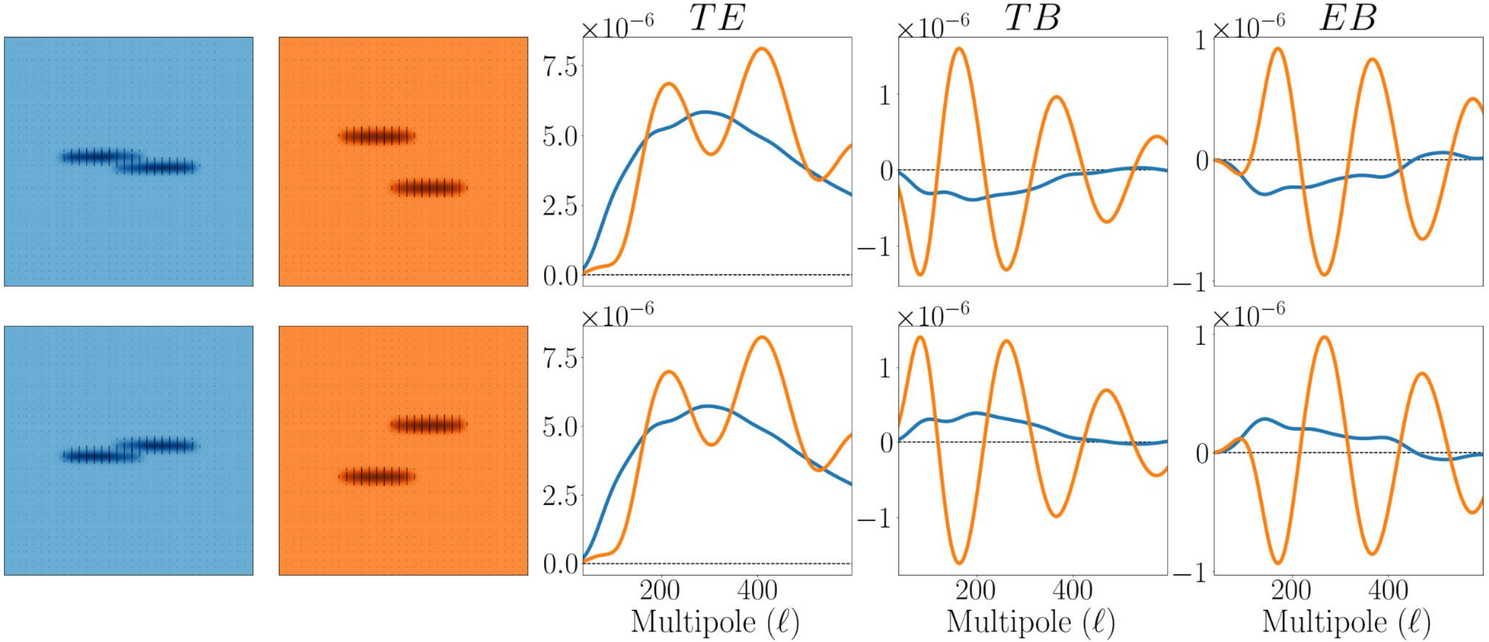

Conclusions

- Separate emission into velocity components
  - Detection in the Galactic component
  - No detection in Magellanic Stream I
- No evidence for decorrelation from inclusion of IVC or between filaments and total dust in the BICEP patch
- Quantify dust sensitivity of different instruments
- Spherical RHT implementation
- Thinnest resolved filaments most informative for magnetic field modeling
- Morphologies producing *TB*, *EB* > 0
- ***B* modes** mostly affected by:
  Filament topologies+polarized intensities wrt one another

  ***E* modes** mostly sensitive to:
  Individual filament shapes

BACKUP

Polarized emission in velocity components

BICEP/Keck Collaboration et al., *ApJ*, 2023

- Detection in the Galactic component of HI → down to 95 GHz
  ~7σ in BB, ~15σ in EE, and ~16σ in EE+BB

- No detection in Magellanic Stream I

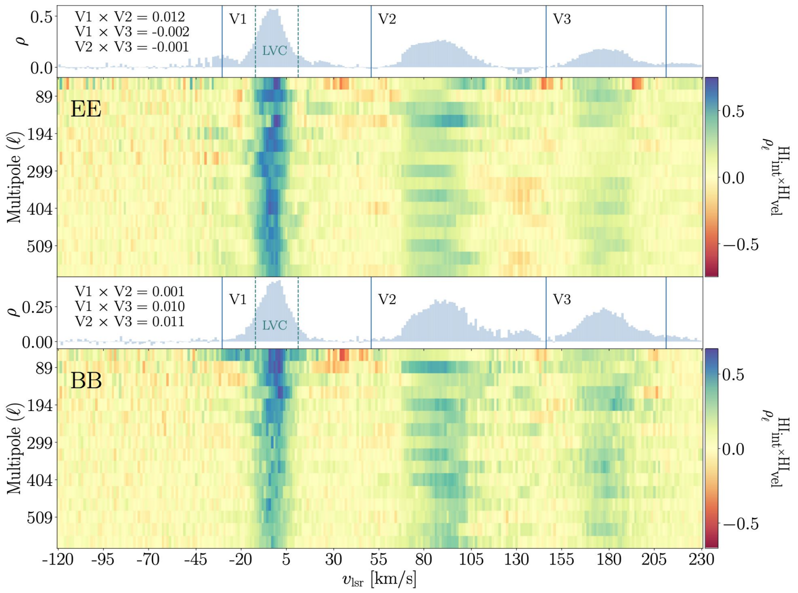

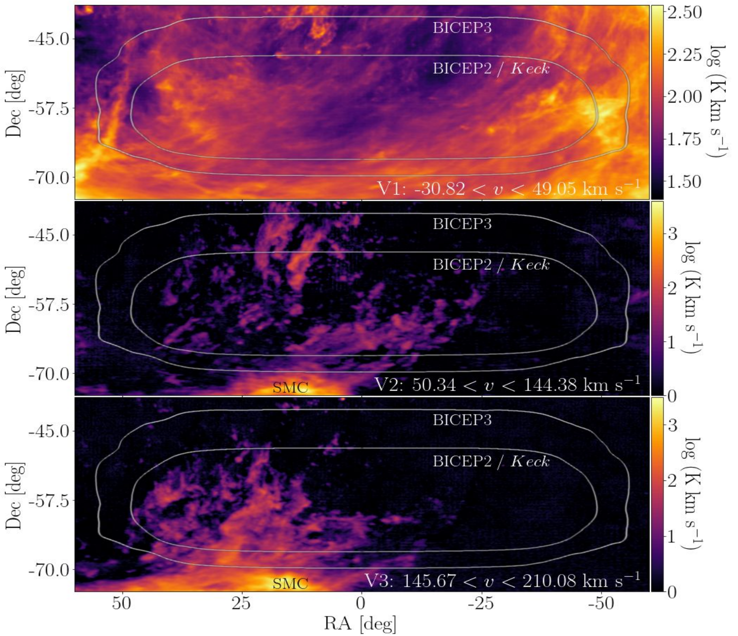

Line-of-sight (LOS) Frequency Decorrelation

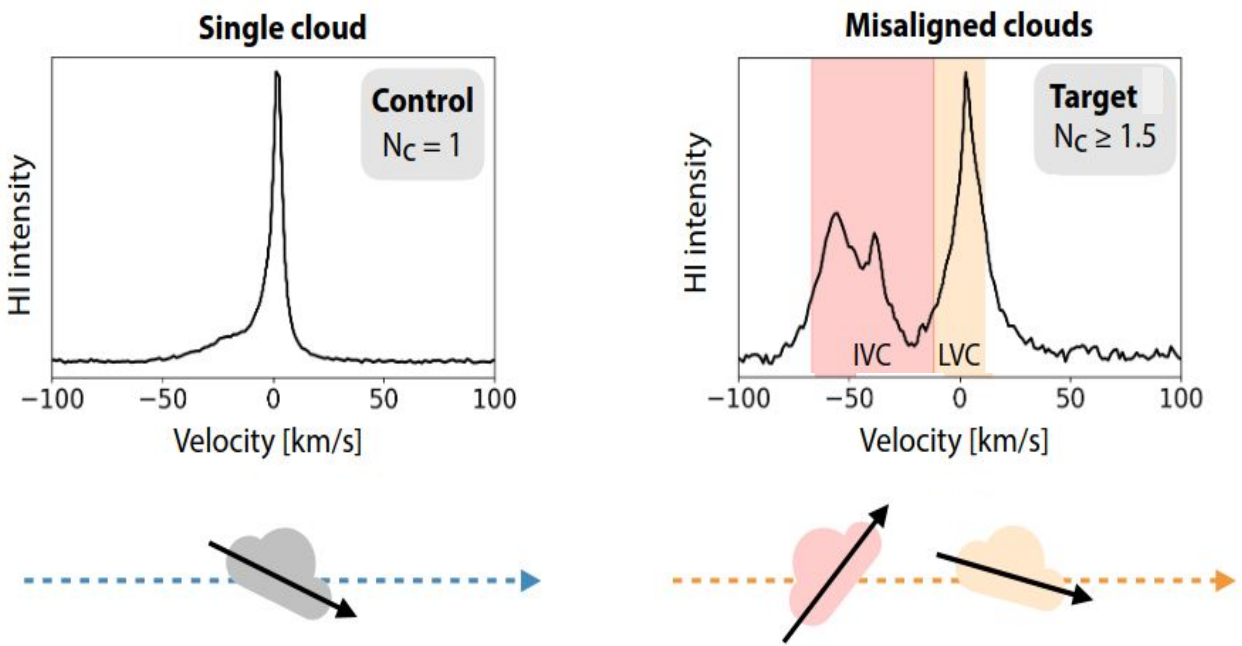

Pelgrims et al. (2021)

- Caused by dust components along the same line-of-sight with different polarization angles and SEDs
- We test for evidence of this phenomenon in the BICEP/*Keck* region between the LVC and IVC components and between the filamentary and total dust components

Inclusion of IVCs in the Line-of-Sight Sum

Detection statistical significance in units of equivalent Gaussian σ's:

	range for LVCs + IVCs	range for LVCs
BB	6.7	6.8
EE	14.6	14.3
$BB + EE$	16.1	16.1

IVC emission integrated over BICEP/*Keck* region ~25% of V1 column in intensity and ~10% in polarized intensity

No change in detection statistical significance

→ No evidence for LOS frequency decorrelation due to inclusion of IVC component in BK patch

Individual Instrument Contributions

Detection statistical significance in units of equivalent Gaussian σ's:

	BB	EE	$BB + EE$
BICEP3 95 GHz	4.53	1.22	4.72
Planck 143 GHz	0.05	0.72	0.12
BICEP2/*Keck* 150 GHz	5.31	2.43	5.98
Planck 217 GHz	3.50	2.37	4.02
Keck 220 GHz	5.82	7.13	9.26
Planck 353 GHz	3.18	7.99	8.59

- Detection at 95 GHz provides a low frequency lever arm for the dust SED
- At lower frequencies, in E modes, we are limited by the sample variance of the CMB

arXiv:2210.05684

- Increase correlation with BICEP/*Keck* and *Planck* by ~2σ in *BB* and ~3σ in *EE* and *EE*+*BB*
- Detection of dust polarization in the Galactic component of HI at ~7σ in *BB*, ~15σ in *EE*, and ~16σ in *EE*+*BB* → down to 95 GHz
- No detection of dust polarization in Magellanic Stream I
- Polarized dust restricted to LVC range → No LOS frequency decorrelation from the inclusion of the IVC component in the BICEP/*Keck* region
- SED through correlations with HI across frequencies → 1.54 ± 0.13 → consistent with BK18 → no evidence for decorrelation between filamentary and total dust in BICEP/*Keck* region

Methodology

- **Sims:**

MBB scaling

$$\tilde{m}_\nu(\hat{\mathbf{n}}, a, k, \beta) = \tilde{m}_\nu^{\Lambda\mathrm{CDM}}(\hat{\mathbf{n}}) + m_\nu^{\mathrm{n}}(\hat{\mathbf{n}}) + a \cdot f_\nu(\beta^{\mathrm{GD}}) \cdot \tilde{m}_\nu^{\mathrm{GD}}(\hat{\mathbf{n}}) + k \cdot f_\nu(\beta^{\mathrm{HI}}) \cdot \tilde{m}_\nu^{\mathrm{HI}}(\hat{\mathbf{n}})$$

Noise

Gaussian dust

- **Observables:**

$$\langle \tilde{m}_\nu(a, k, \beta^{\mathrm{HI}})\ \tilde{m}_\nu^{\mathrm{HI}} \rangle_X = \langle \tilde{m}_\nu^{\Lambda\mathrm{CDM}}\ \tilde{m}_\nu^{\mathrm{HI}} \rangle_X + \langle m_\nu^{\mathrm{n}}\ \tilde{m}_\nu^{\mathrm{HI}} \rangle_X + a \cdot f_\nu(\beta^{\mathrm{GD}}) \cdot \langle \tilde{m}_\nu^{\mathrm{GD}}\ \tilde{m}_\nu^{\mathrm{HI}} \rangle_X + k \cdot f_\nu(\beta^{\mathrm{HI}}) \cdot \langle \tilde{m}_\nu^{\mathrm{HI}}\ \tilde{m}_\nu^{\mathrm{HI}} \rangle_X$$

- **Likelihood:**

vector across X, ν, ℓ

$$\chi^2(a, k, \beta) \equiv \left(\mathbf{D}^{\mathrm{real}} - \overline{\mathbf{D}}(a, k, \beta)\right)^{\mathrm{T}} \mathbf{M}^{-1} \left(\mathbf{D}^{\mathrm{real}} - \overline{\mathbf{D}}(a, k, \beta)\right)$$

- **Detection statistical significance:**

Null hypothesis: $\chi^2_{\mathrm{GD}}(a) \equiv \chi^2(a, 0, 0)$ → added benefit of HI: $\Delta\chi^2 = \hat{\chi}^2_{\mathrm{GD}} - \hat{\chi}^2$ → PTE (p-value) → inv. normal → σ

Polarized Intensity

- Results insensitive to RHT parameters, as long as in regime where longer structures are selected
- *BB* correlation breaks down when less filamentary structure is admitted to the model
- Further explorations of physical implications of this parameter space in a separate paper

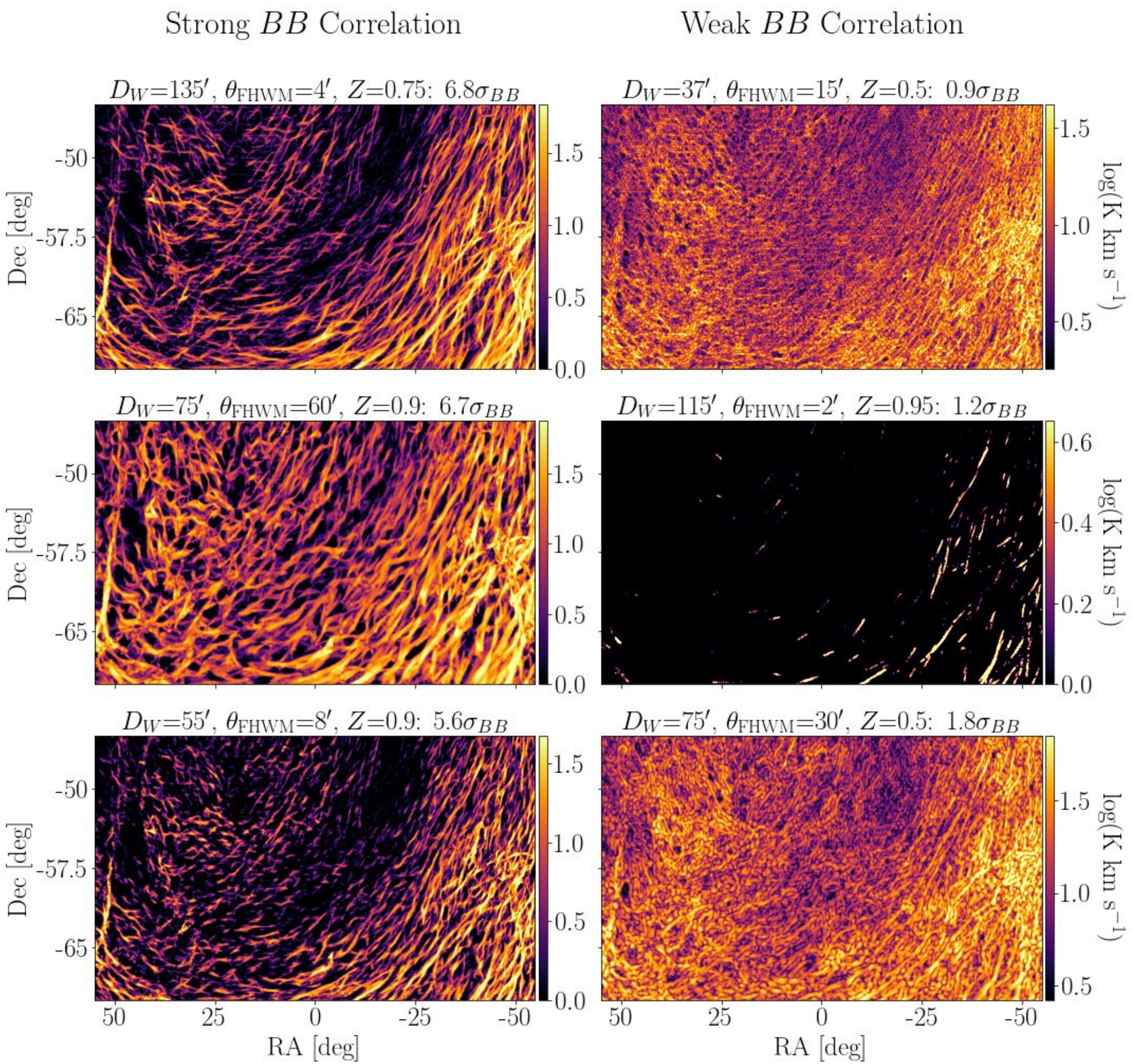

RHT Parameter Tuning

Detection statistical significance in units of equivalent Gaussian σ's:

	$D_W = 75'$, $\theta_{FWHM} = 30'$, $Z = 0.7$	$D_W = 135'$, $\theta_{FWHM} = 4'$, $Z = 0.75$
	default	best
BB	4.7	6.7
EE	12.3	14.6
$BB + EE$	12.9	16.1

(used in Clark & Hensley 2019)

Uncertainties (from fits of 499 realizations with fixed inputs)

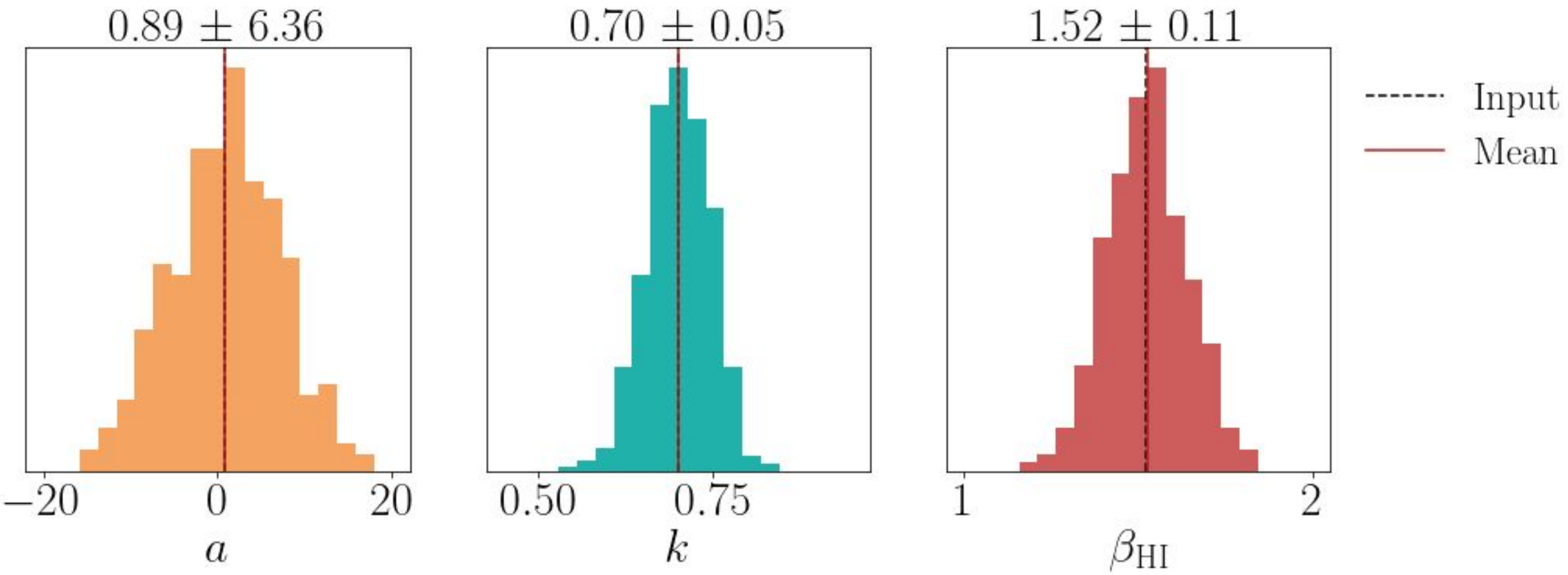

Mean consistent with input → fits are unbiased

Best-Fit Observables

Cross-correlations with the real data highly exceed the spurious correlations across all frequencies

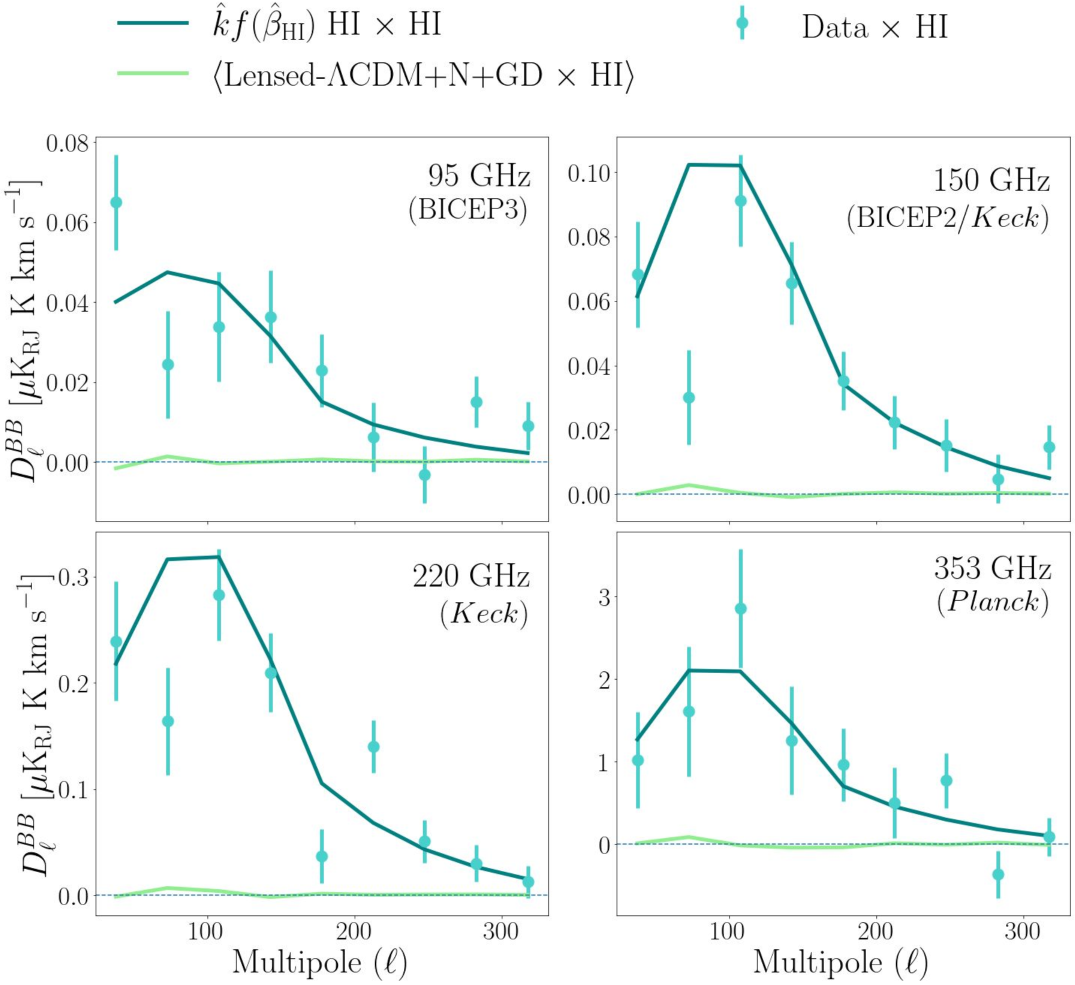

Posteriors

(Uniform Priors, χ^2 Likelihood)

Fitting HI auto spectra to cross spectra between HI and dust across frequencies

- ***k*:** more standard deviations from 0 → more detection (value folds in HI normalization)
- $\boldsymbol{\beta_{HI}}$: SED spectral index. *E* and *B* modes are sourced by the same filaments in HI template

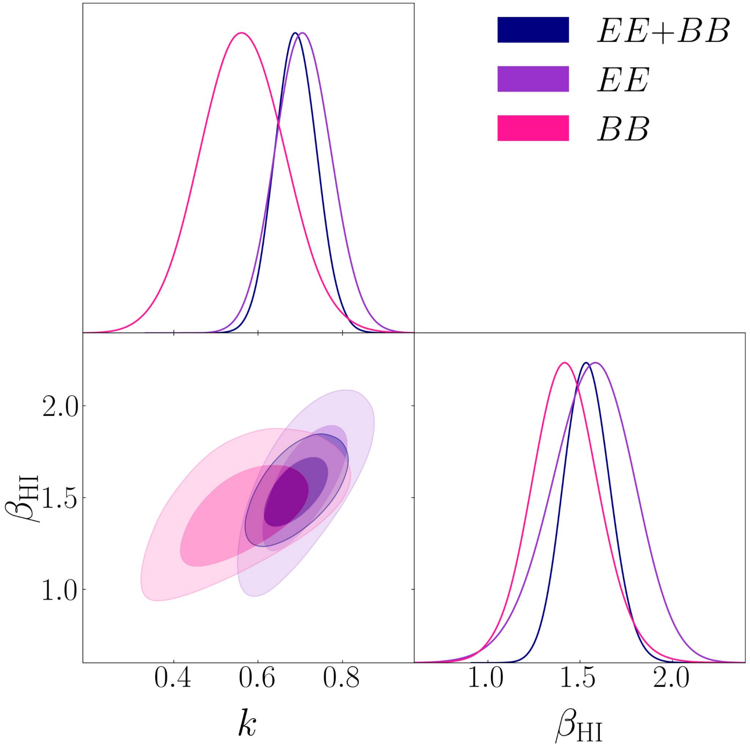

Change in SED with Frequency Channel Omissions

- *Planck*'s 143 and 217 GHz bands are not very sensitive to filamentary dust polarization when restricted to the BICEP/*Keck* region as compared to BICEP/*Keck*'s 150 and 220 GHz bands → *Planck*-only case has a wider posterior that is shifted slightly towards higher values of $\beta_{\rm HI}$

- The four posteriors are statistically consistent with each other to within 2σ

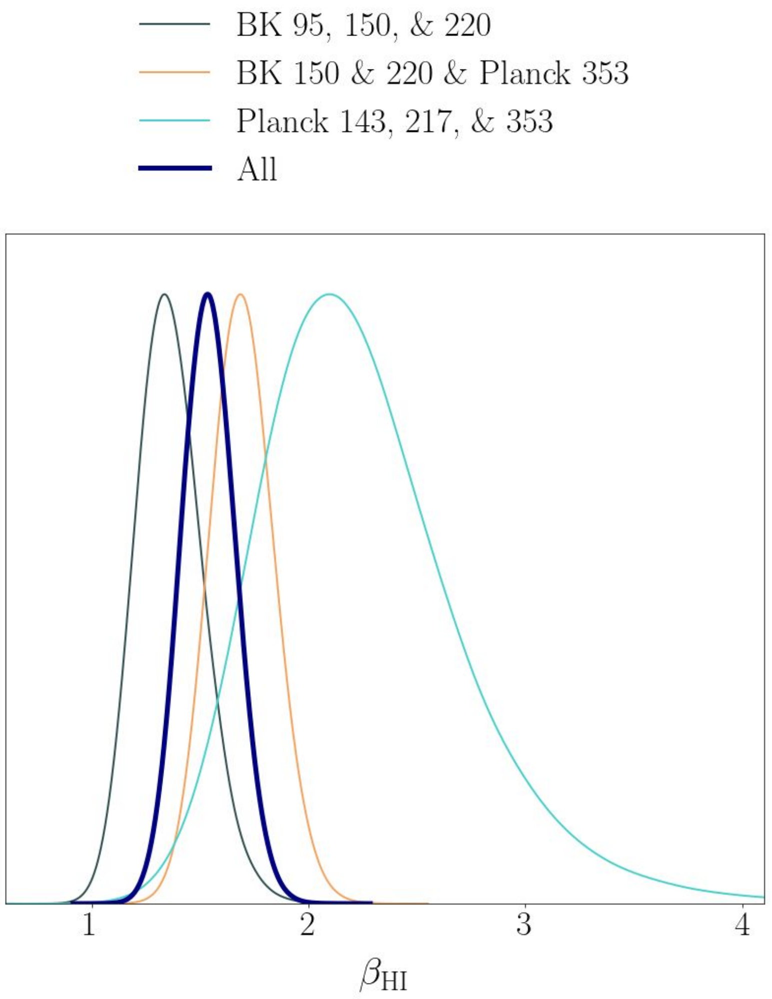

Correlation Ratios

- Auto spectra in denominator contain noise biases → For the purposes of forecasting sensitivity to *r*, we wish to retain the diluting effects of noise

- BICEP/*Keck* bands correlate better in *B* modes than *Planck* bands of similar frequencies in this region (consistent with BK18)

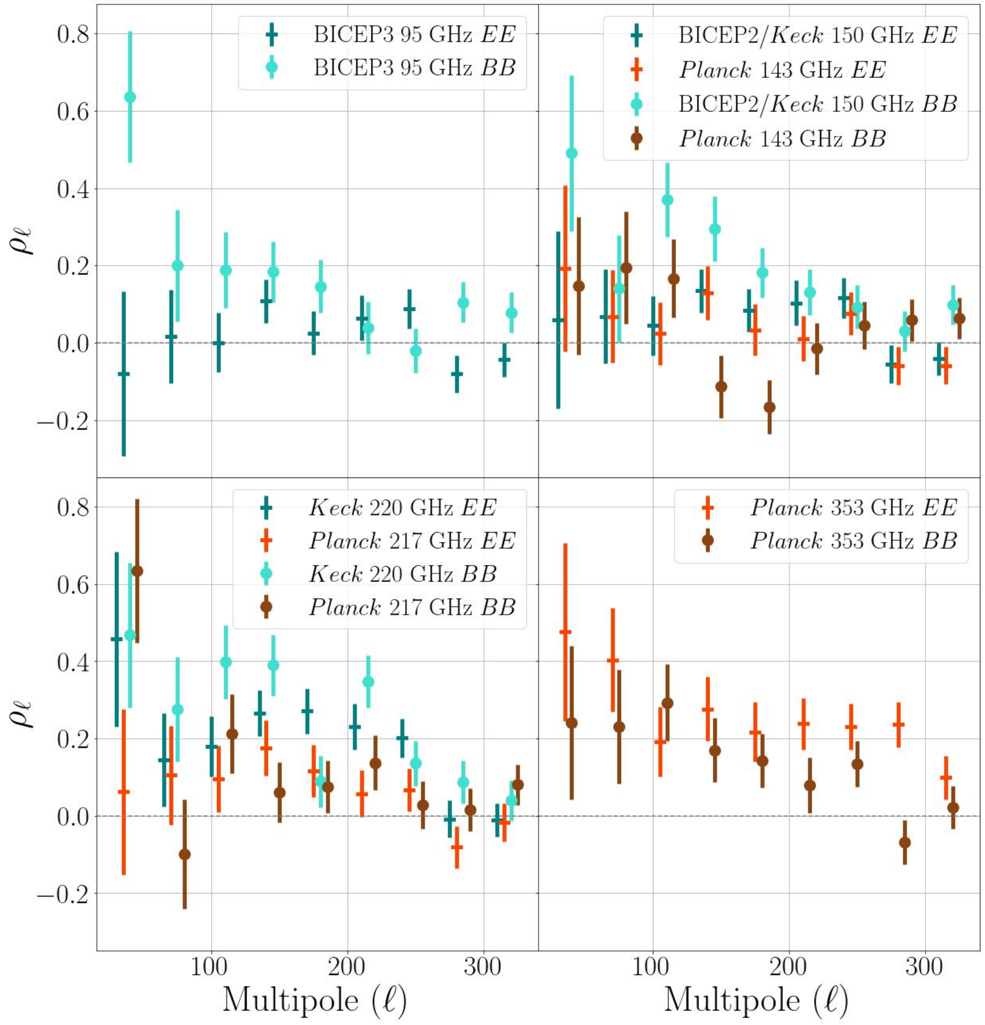

Cross Spectra

- BICEP/*Keck* bands correlate better in *B* modes than *Planck* bands of similar frequencies in this region (consistent with BK18)

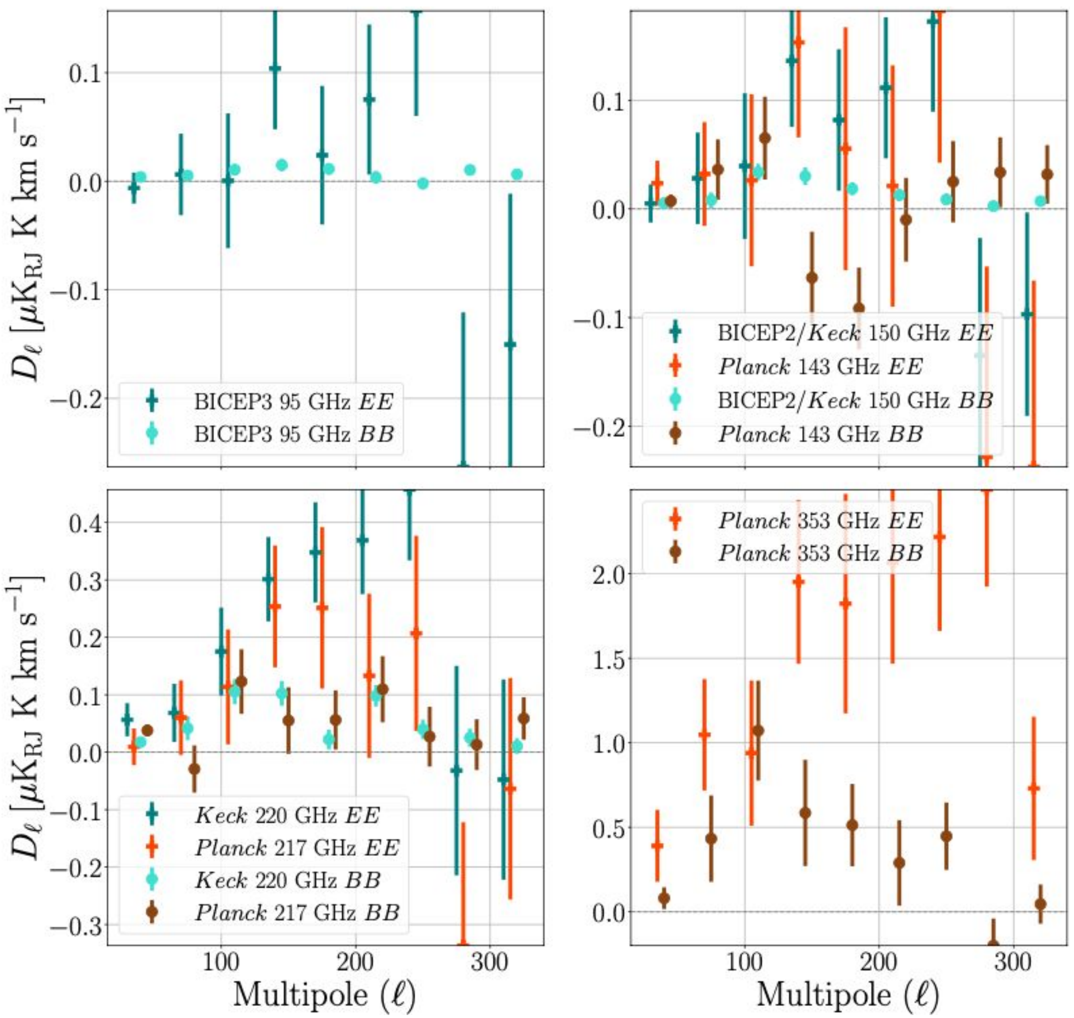

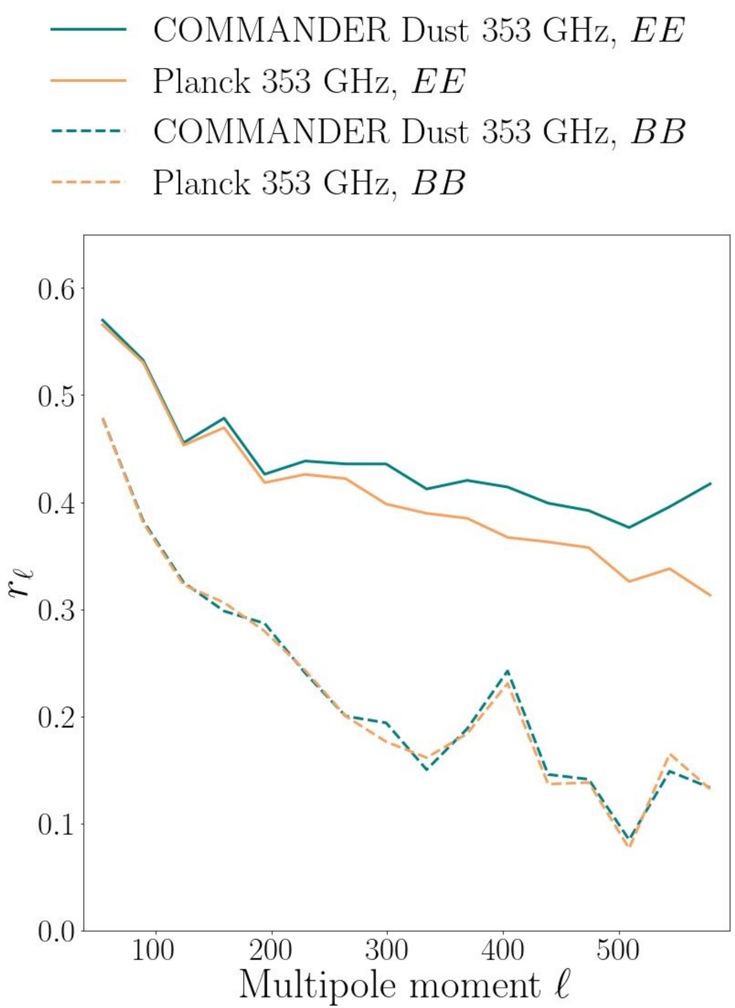
COMMANDER Dust 353 GHz, EE
Planck 353 GHz, EE
COMMANDER Dust 353 GHz, BB
Planck 353 GHz, BB
0.6
0.5
0.4
r_ℓ
0.3
0.2
0.1
0.0
100
200
300
400
500
Multipole moment ℓ

Higher-resolution HI

Halal, Clark, Cukierman, Beck, & Kuo, submitted to *ApJ*, 2023

~10% enhancement in *B*-mode correlation

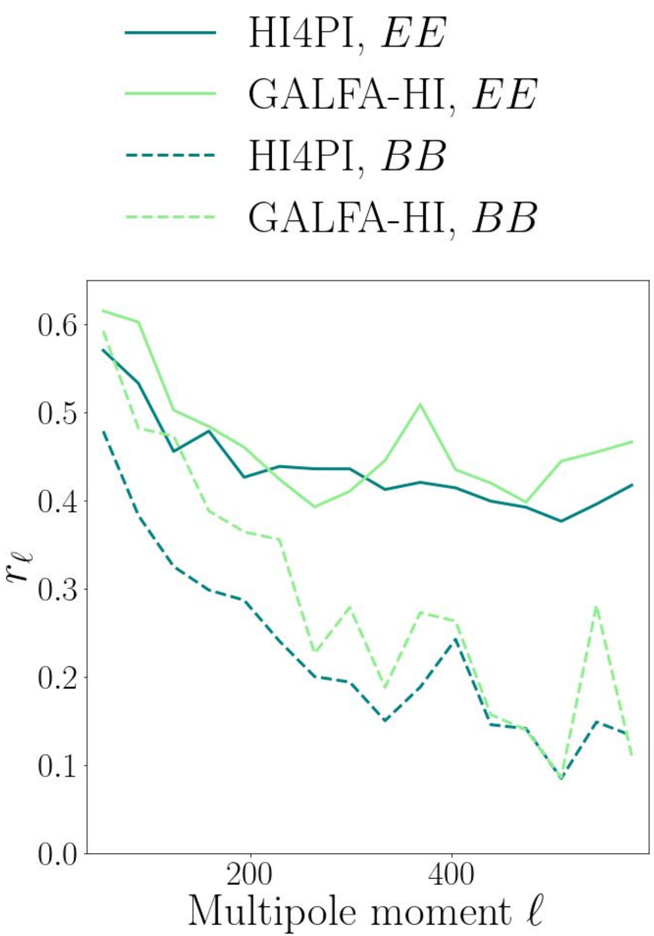

Compare outputs to Hessian-based method

Halal, Clark, Cukierman, Beck, & Kuo, submitted to *ApJ*, 2023

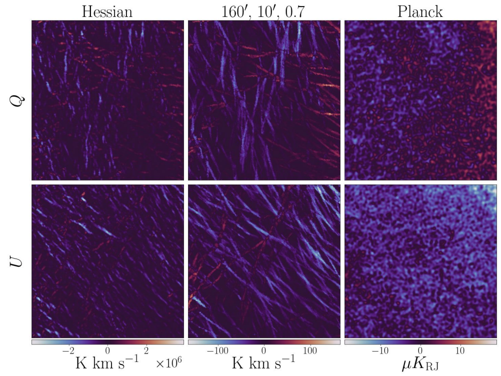

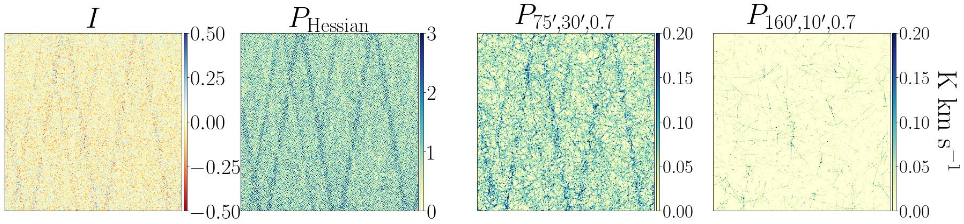

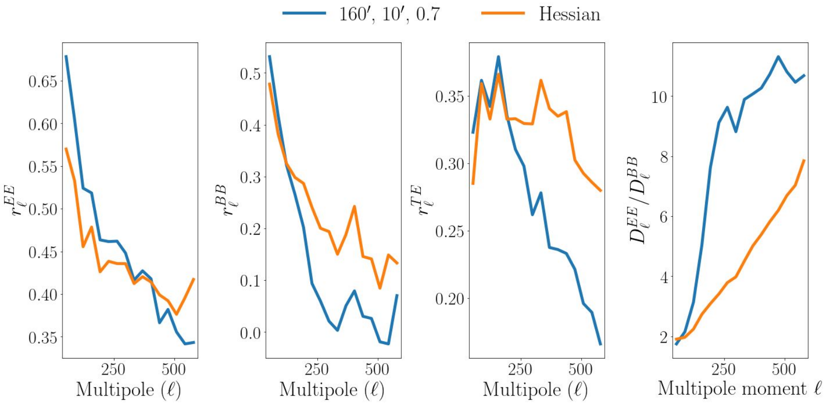

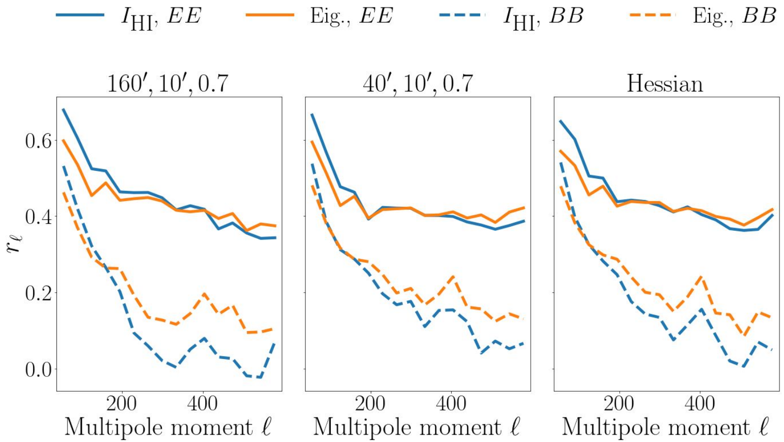

Improvements to template construction

Halal, Clark, Cukierman, Beck, & Kuo, submitted to *ApJ*, 2023

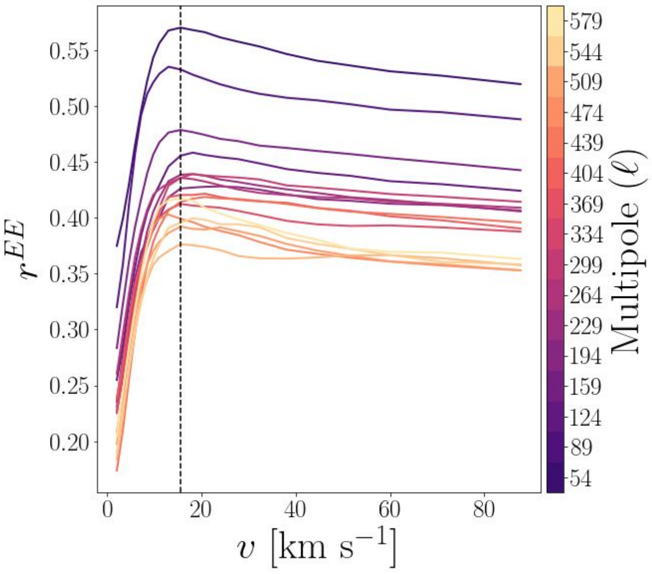

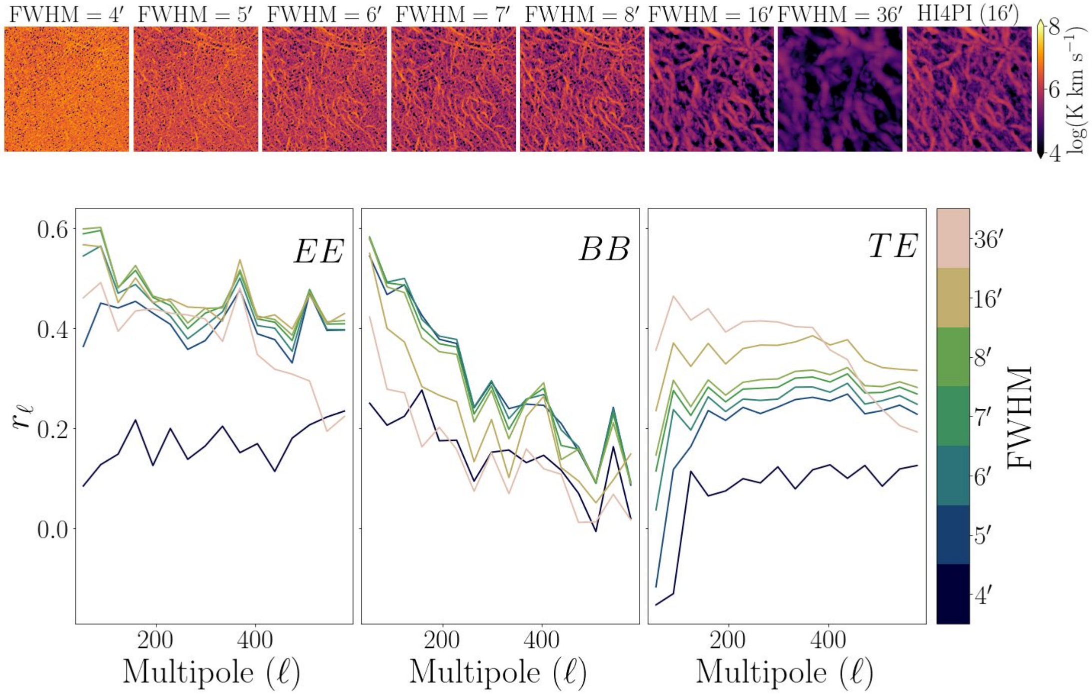

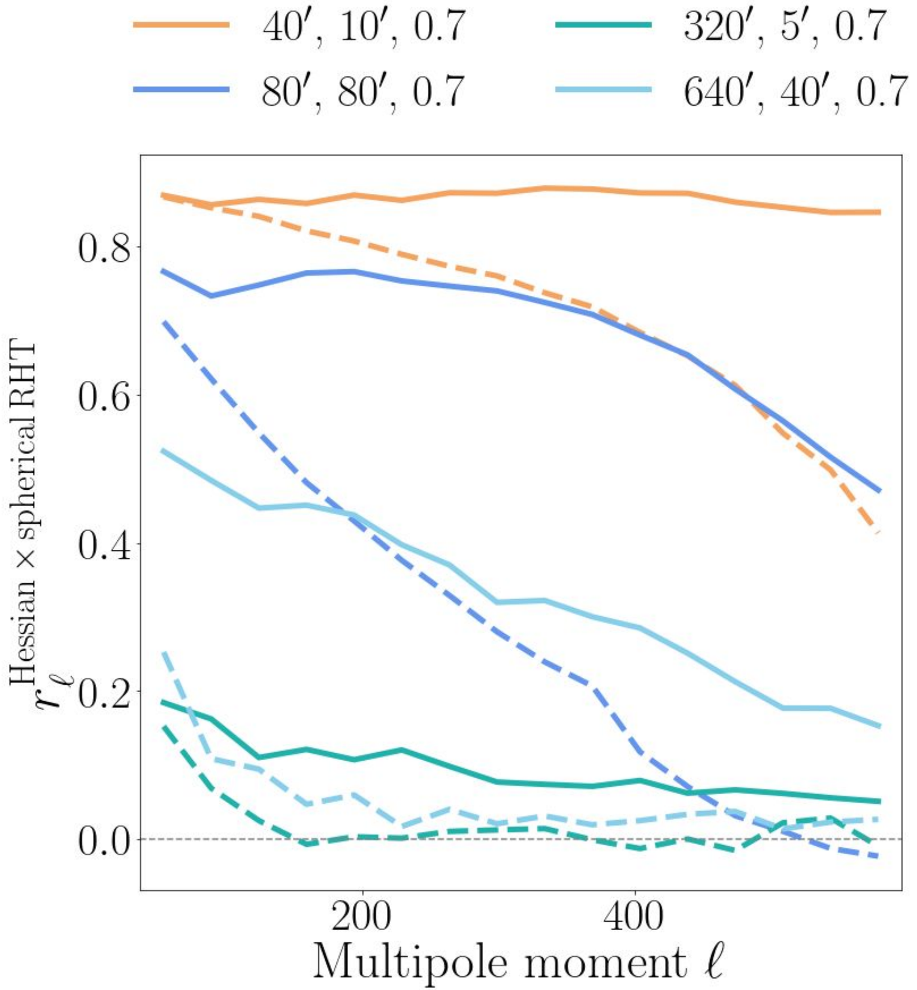
40′, 10′, 0.7
320′, 5′, 0.7
80′, 80′, 0.7
640′, 40′, 0.7
$r_\ell^{\mathrm{Hessian} \times \mathrm{spherical\,RHT}}$
0.0
0.2
0.4
0.6
0.8
200
400
Multipole moment ℓ

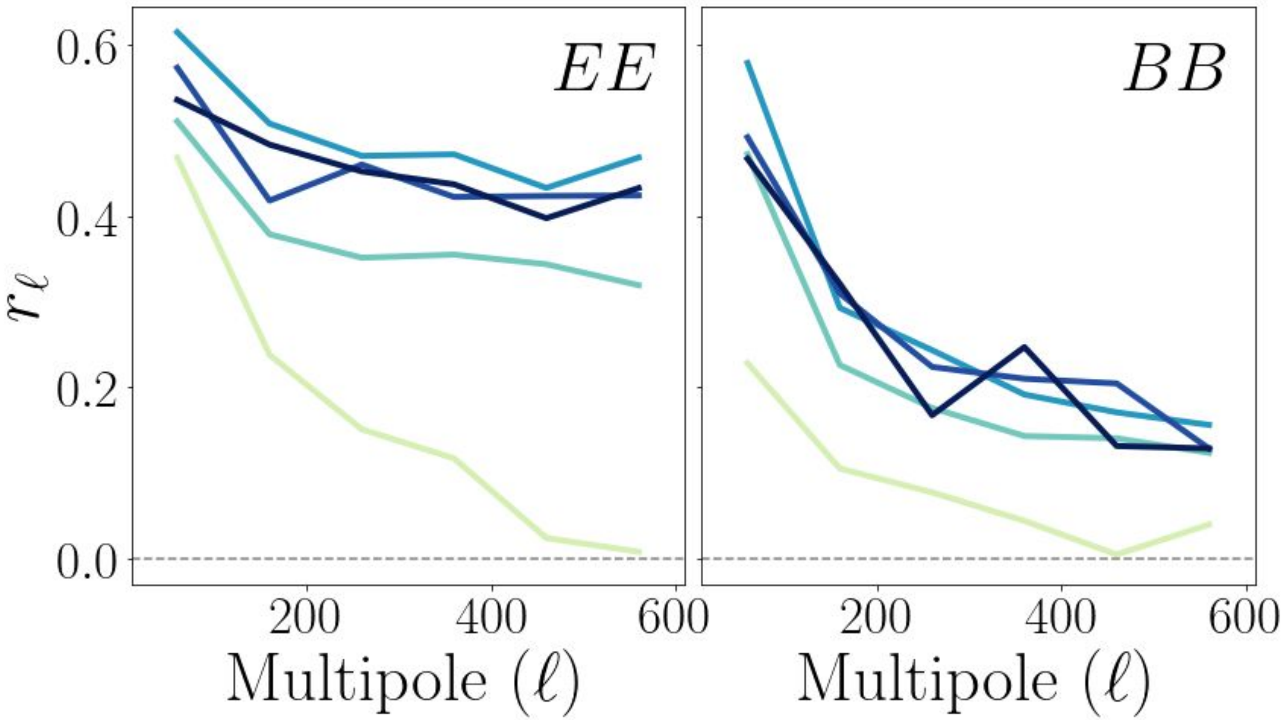
EE
BB
r_ℓ
0.0
0.2
0.4
0.6
200
400
600
Multipole (ℓ)
200
400
600
Multipole (ℓ)

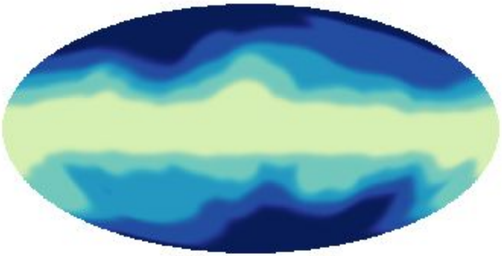

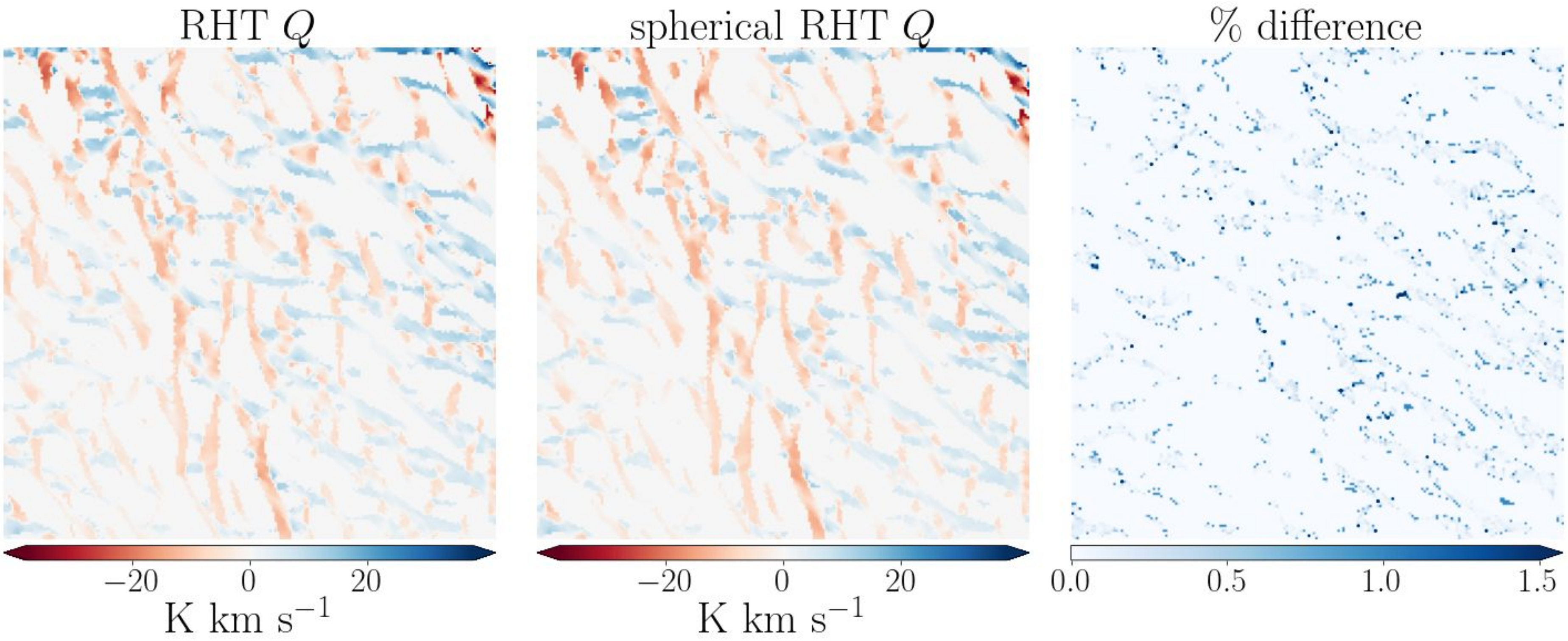
RHT Q
spherical RHT Q
% difference
−20
0
20
K km s^{-1}
−20
0
20
K km s^{-1}
0.0
0.5
1.0
1.5